Matrix Viscoelasticity Decouples Bubble Growth and Mobility in Coarsening Foams

Chiara Guidolin,[1,2,*] Emmanuelle Rio,[1] Roberto Cerbino,[3] Fabio Giavazzi,[2,†] and Anniina Salonen[1,‡]
[1]Université Paris-Saclay, CNRS, Laboratoire de Physique des Solides, Orsay, France
[2]Department of Medical Biotechnology and Translational Medicine, University of Milan, Segrate, Italy
[3]Faculty of Physics, University of Vienna, Vienna, Austria

(Received 9 December 2023; revised 3 May 2024; accepted 15 July 2024; published 21 August 2024)

Pressure-driven coarsening triggers bubble rearrangements in liquid foams. Our experiments show that changing the continuous phase rheology can alter these internal bubble dynamics without influencing the coarsening kinetics. Through bubble tracking, we find that increasing the matrix yield stress permits bubble growth without stress relaxation via neighbor-switching events, promoting more spatially homogeneous rearrangements and decoupling bubble growth from mobility. This eventually leads to a structural change that directly impacts the foam mechanical and stability properties, essential for applications in various technological and industrial contexts.

DOI: 10.1103/PhysRevLett.133.088202

Liquid foams are soft materials made of gas bubbles tightly packed together in a continuous liquid medium. Such systems can age through pressure-driven gas transfer between the bubbles, which results in a gradual growth of the mean bubble size [1]. This coarsening process induces internal stress-driven dynamics: bubble size variations give rise to imbalanced stresses inside the foam, which eventually relax through local bubble rearrangements entailing an exchange of neighbors [2]. Probing the link between restructuring events and the coarsening process in model systems like foams can shed a light on the interplay between stress accumulation, local yielding, and structural relaxation that is common to a variety of other soft glassy systems [3].

Bubble dynamics has been widely probed in coarsening aqueous foams with light scattering techniques [4–7]. The frequency of rearrangements is set by the strain rate imposed by the coarsening process, thus it is directly linked to the coarsening rate [7]. A combination of reciprocal and direct space analysis has more recently shown how coarsening dynamics is governed by directionally persistent bubble displacements up to a critical length scale given by the bubble size [8]. The loss of persistency has been ascribed to sudden changes in the local stress configuration due to the occurrence of plastic bubble rearrangements inside the foam.

While all this holds for aqueous foams, many practical applications involve foams made from more complex fluids, like gels, emulsions, or pastes. The behavior and characteristics of these types of foams are considerably less understood. How easily bubbles can move during coarsening clearly depends on the amount, as well as on the nature of the medium between them [6]. Both surface and bulk rheology of the continuous phase significantly affect the duration of plastic events within the foam. For instance, increased interfacial and bulk viscosity both translate into slower rearrangements [9]. By contrast, the effect of elastic properties has been scarcely investigated. Conditions required for preventing or arresting coarsening have been proposed with high foam elasticity [10] or continuous phase yield stress [11,12]. However, a thorough description of the impact of bulk elasticity on coarsening dynamics is still missing. Recently, spatially heterogeneous coarsening has been observed in foams with viscoelastic continuous phases, eventually leading to atypical foam morphologies [13]. Establishing the link between coarsening dynamics and structural evolution in complex foams would thus allow for a finer control of internal foam structure, which is crucial for applications, but still calls for a systematic investigation of how bubble motion changes with matrix stiffness.

In this Letter, we experimentally investigate how the presence of a viscoelastic medium between the bubbles affects their mobility during coarsening. By performing bubble tracking, we show that a gradual increase of the continuous phase yield stress dramatically restricts bubble motion during coarsening. Moreover, we show that the marked change in the bubble dynamics is not mirrored by a significant change in the coarsening kinetics, suggesting a decoupling between the coarsening rate and the rate of restructuring events inside the foam.

We follow the ageing of foams made of concentrated oil-in-water emulsions, as sketched in Fig. 1(a). At oil volume fractions ϕ above random close packing, emulsions have a storage modulus and a yield stress both increasing with

*Contact author: chiara.guidolin@unimi.it
†Contact author: fabio.giavazzi@unimi.it
‡Contact author: anniina.salonen@universite-paris-saclay.fr

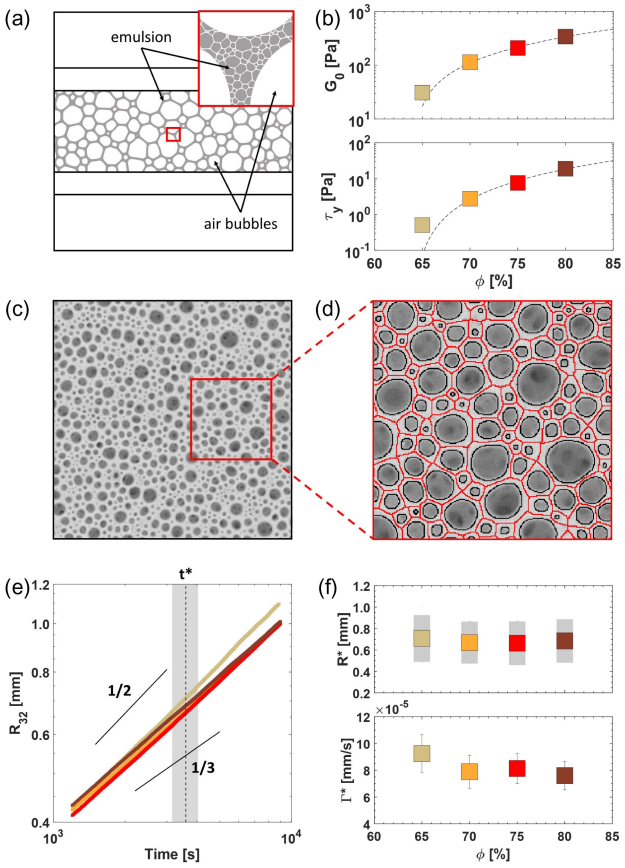

FIG. 1. Foam coarsening in concentrated emulsions. (a) Illustration of the foam sample, highlighting the oil-in-water emulsion between the bubbles. (b) Emulsion storage modulus G_0 (top) and yield stress τ_y (bottom) at different ϕ. Experimental details can be found in [13]. The dashed lines represent the two expected scalings $G_0 \sim \phi(\phi - \phi^*)$ [14] and $\tau_y \sim (\phi - \phi^*)^2$ [15], where $\phi^* = 64\%$. (c) Top view of a foam at $\phi = 75\%$ at $t^* = 60$ min. The frame edge is 30 mm. (d) Enlargement showing the outline of the bubble segmentation (black) and the associated foam skeleton (red). The frame edge is 10 mm. (e) Mean bubble growth at different ϕ. The gray-shaded area highlights the time window considered, centered around $t^* = 60$ min (vertical dashed line). (f) Mean bubble size and coarsening rate evaluated at $t = t^*$. The gray-shaded bars on R^* represent the standard deviation of the bubble size distribution.

ϕ [14,15]. We consider oil fractions ranging between 65% and 80%, so that we vary the elastic modulus of the foam continuous phase G_0 between 30 and 340 Pa, and its yield stress τ_y from 0.5 to 20 Pa, as shown in Fig. 1(b). In this range of ϕ, the emulsion yield stress delays the gravitational drainage [16] allowing the foam to coarsen at homogeneous liquid fraction [17].

Emulsions are first prepared at the desired ϕ by mixing rapeseed oil (from Brassica rapa, Sigma Aldrich) and an aqueous surfactant solution (sodium dodecyl sulphate 30 g/L, Sigma Aldrich) with the double-syringe method [25], and then foamed with the aid of a planetary kitchen mixer until the sample volume has increased tenfold (liquid fraction ranging between 9% and 11%). The resulting foam is then gently sandwiched between two square glass plates (edge 20 cm), separated by a 10 mm thick square rubber gasket. The spacing is thus much larger than the typical bubble size ($R \sim 10^{-1}$ mm) so that the foam sample can be safely considered three-dimensional. The typical bubble Laplace pressure ($\gamma/R \simeq 300$ Pa with $\gamma \simeq 30$ mN/m) is higher than the interstitial emulsion yield stress, ensuring that our foams coarsen [11,12].

Foam ageing is monitored from the top by taking image stacks with a camera (Basler acA3800-14um, equipped with a Tamron lens 16 mm $F/1.4$), while a square array of LED lights provides uniform illumination from above. The typical foam appearance is shown in Fig. 1(c). Image processing is performed with custom MATLAB scripts as follows. Foam pictures are first segmented through an adaptive thresholding and then skeletonized with a watershed algorithm. An example of bubble segmentation and foam skeleton outline is shown in Fig. 1(d). From the foam skeleton, we estimate the size of each bubble as the radius $R = \sqrt{A/\pi}$, where A is the area of the polygonal cell, to then monitor how its average value, taken as $R_{32} = \langle R^3 \rangle / \langle R^2 \rangle$, evolves over time. The time evolution of R_{32} at different ϕ is reported in Fig. 1(e): despite the tenfold increase in the emulsion elasticity, the mean bubble growth is approximately the same for each sample over almost one decade in time. At the liquid fractions considered (~10%), neighboring bubbles share thin liquid films, whose surface area is however reduced by the presence of thick Plateau borders. Interbubble gas diffusion is thus slower than in a dry foam (liquid fraction ~1%) with the same skeleton [26]. The experimental curves of $R_{32}(t)$ indeed lie between the two power laws predicted for the mean bubble growth in very dry foams [27] and dilute bubbly liquids [28] in their scaling state (SM, Fig. S2). However, in contrast to aqueous foams, the foams under study are not expected to head toward self-similarity. In fact, lack of liquid phase redistribution and a nontrivial interplay between foam structure and rheology has been shown to eventually lead to highly heterogeneous structures at millimetric bubble sizes [13].

We now compare the coarsening dynamics at the same foam age t^*. We present here data for $t^* = 60$ min, but choosing different values of t^* does not affect the final results (SM, Sec. 1). The mean bubble size $R^* = R_{32}(t^*)$ and its growth rate $\Gamma^* = \mathrm{d}R_{32}/\mathrm{d}t|_{t^*}$ show no significant dependence on ϕ, as shown in Fig. 1(f). The bubble size distribution also does not change with ϕ (SM, Fig. S3).

However, a visual inspection of the coarsening movies reveals a dramatic change in the global bubble dynamics with increasing ϕ (SM, movies SM1–SM4). At $\phi = 65\%$, bubbles freely rearrange as they coarsen, as in an aqueous foam. By contrast, as ϕ is increased up to 80%, their

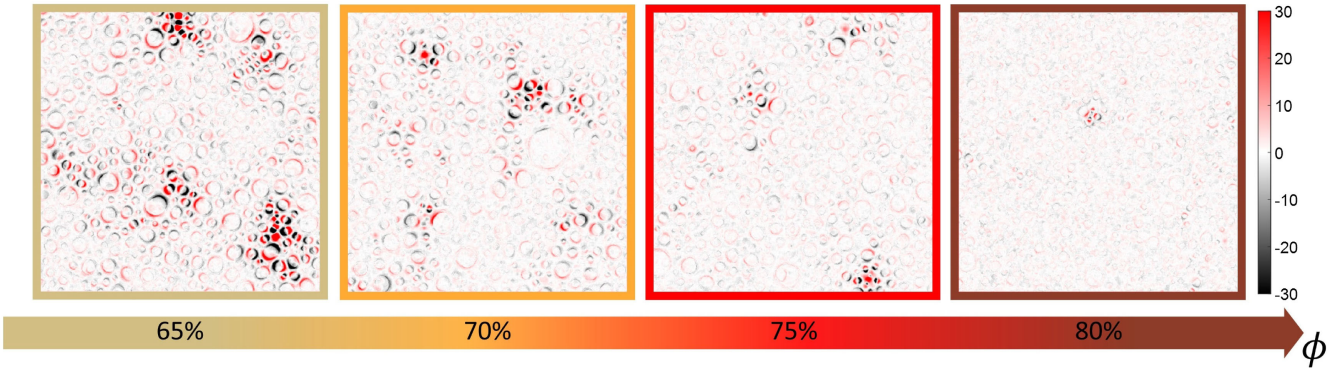

FIG. 2. Activity maps. Representative activity maps of coarsening foams at increasing ϕ, compared at the same foam age $t^* = 60$ min. The maps are obtained as the difference between two frames separated by $\Delta t = 60$ s. The frame edge is 25 mm. The colormap corresponds to the difference in the grayscale level of the images, as indicated by the colorbar.

mobility is drastically reduced: bubbles appear to just grow or shrink while remaining substantially stuck in their initial positions.

The different bubble dynamics can be better appreciated with the aid of activity maps like the ones shown in Fig. 2. The higher activity of the foam at $\phi = 65\%$ stands out at first glance. Here, we recognize the occurrence of topological changes as the regions where two couples of red and black sickle areas emerge symmetrically, marking the neighbor-switching event. Furthermore, these plastic events cause substantial motion in the surrounding bubbles, extending up to 4–5 bubbles away, as in aqueous foams [5,7]. On the other hand, as ϕ is increased, bubble rearrangements rarefy (SM, Fig. S8,S9) and the overall activity is drastically reduced.

We characterize such differences in the coarsening dynamics by tracking the bubbles. Since foams are aging, the bubble size, the coarsening rate, and the bubble mobility are all systematically changing over time. To limit the global bubble growth while tracking the bubble trajectories, we thus restrict the analysis to an image subsequence covering a 15-min time window centered around $t = t^*$, as highlighted in Fig. 1(e), that ensures a variation in the mean bubble size of less than 15% for each ϕ. This allows studying bubble dynamics in quasistationary conditions [8].

We perform bubble tracking by using TrackMate [29,30] on the segmented foam pictures. The results obtained at $\phi = 65\%$ and $\phi = 80\%$ are reported in Fig. 3(a), where examples of representative trajectories are shown for both samples.

At $\phi = 65\%$, bubbles move persistently in one direction until a sudden deviation occurs, as mirrored by the jumps in the bubble trajectories. Such abrupt changes of direction are not observed at $\phi = 80\%$ where, by contrast, trajectories are straighter and shorter [17]. In aqueous foams, the loss of directional persistency has been ascribed to the change in the local stress configuration after the occurrence of plastic bubble rearrangements in the surroundings [8]. This agrees with our observations: while at low ϕ bubbles rearrange during coarsening, at high ϕ mutual bubble displacements are almost suppressed (SM, Fig. S9).

To quantify these observations, we compute the probability distribution of bubble displacements Δr at different time delays Δt (i.e., the self part of the Van Hove correlation function [31]). For each ϕ, the distribution exhibits a well-defined peak at each time delay, that systematically shifts toward larger Δr as Δt is increased, as shown in Fig. 3(b) for $\phi = 65\%$ and $\phi = 80\%$. Results for the other values of ϕ can be found in Supplemental Material (Fig. S2). At $\phi = 65\%$, the right tail of the distribution decreases as a power law before dropping at Δr around the characteristic bubble size, akin to aqueous foams [8]. By contrast, at $\phi = 80\%$ the distributions decay more steeply and displacements are restricted to smaller length scales.

We compute the bubble mean square displacement $\mathrm{MSD} = \langle \Delta r^2 \rangle$ at different time delays for each sample. For this calculation, we discard small bubbles whose trajectories do not cover the whole time window, which correspond to less than 20% of the total number of detected bubbles. The MSD dependency on Δt is plotted in Fig. 3(c) for each ϕ. The MSD grows asymptotically as a power law $\mathrm{MSD} \sim \Delta t^{\delta}$, with an exponent δ increasing with ϕ, heading toward a ballistic-like scaling.

Despite the same coarsening rate, for a fixed Δt the MSD shows a tenfold reduction as ϕ is increased from 65% to 80%, reflecting shorter bubble displacements with increasing emulsion elasticity. The average bubble size can thus grow in the same way, with very different bubble dynamics. Changing the continuous phase rheology allows switching from traditional foam coarsening to a new coarsening where mutual bubble displacements are hindered. The MSD approaching a ballistic scaling at high ϕ indeed reflects the bubble tendency to keep moving persistently (SM, Fig. S7), which is a signature of the loss of plastic bubble rearrangements (SM, Fig. S9).

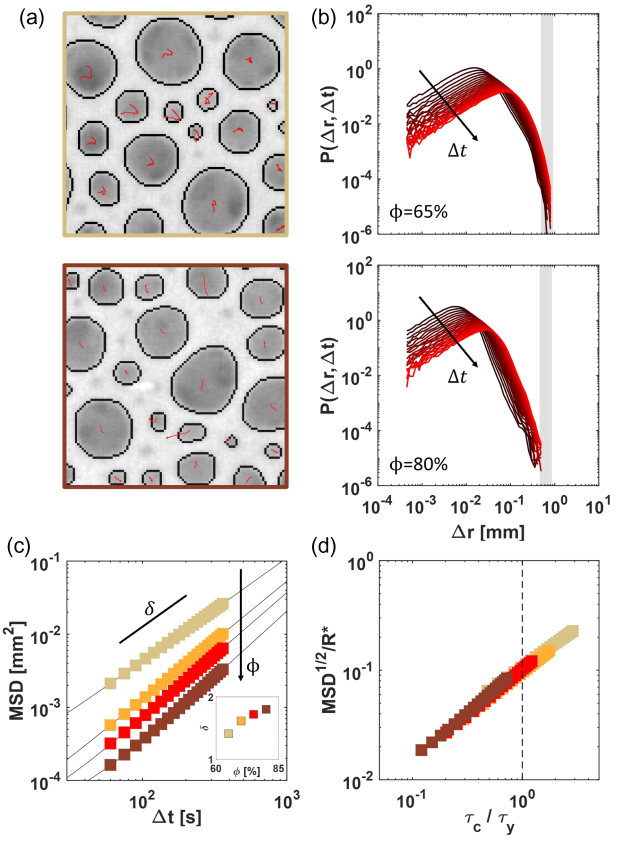

FIG. 3. Bubble tracking. (a) Representative bubble trajectories, lasting the whole time window, obtained at $\phi = 65\%$ (top) and $\phi = 80\%$ (bottom). The frame edge is 4 mm. (b) Distribution of bubble displacements at different Δt (increasing from 60 to 360 s with a step of 15 s) for $\phi = 65\%$ and $\phi = 80\%$. The vertical gray-shaded bar marks the mean bubble radius R^*. (c) Bubble mean square displacement as a function of Δt. MSD $\sim \Delta t^{\delta}$ for each sample, with δ increasing with ϕ, as shown in the inset. (d) MSD rescaling. The dashed line marks $\tau_c = \tau_y$.

The change in the bubble dynamics can be traced back to the continuous phase rheology. The emulsion elasticity allows considering the foam continuous phase as a soft elastic solid for small deformations [10]. The diffusive gas exchange between neighboring bubbles induces a variation in their size, which generates an elastic deformation of the matrix. Bubble size variations hence give rise to local elastic stresses that tend to restore the initial unstrained structure. While coarsening, the foam can thus accumulate stress in the matrix due to the change in the bubble packing conditions. As the strain rate associated to the coarsening process can be written as Γ^*/R^* [7,8], we estimate the total strain applied to the system in a given time Δt as $(\Gamma^*/R^*)\Delta t$, and the total stress accumulated by the foam as $\tau_c = (\Gamma^*/R^*)\Delta t G_0$, where G_0 is the elastic modulus of the matrix. Once this stress overcomes the emulsion yield stress, it can relax via local plastic bubble rearrangements. Indeed, in order for bubbles to rearrange, the emulsion in the Plateau borders has to yield. On the other hand, as ϕ is increased, the interstitial emulsion can bear higher stresses without yielding. We thus compare τ_c with τ_y by plotting the normalized average displacement $\mathrm{MSD}^{1/2}/R^*$ versus the relative stress τ_c/τ_y. As shown in Fig. 3(d), data display a good collapse. Results obtained at different foam ages also collapse on the same master curve [SM, Fig. S3(d)], meaning that coarsening-driven bubble displacements are set by how much stress the emulsion can bear without yielding. At high ϕ the emulsion between the bubbles is stiff enough to elastically store the stress due to bubble size variations and counteract bubble rearrangements. Only when τ_c equals τ_y has the system accumulated enough stress to yield the emulsion so that bubbles can rearrange.

Since the mutual bubble displacement is of the order of $\mathrm{MSD}^{1/2}$ and the typical interbubble distance is of the order of the bubble size R^*, we can think of $\mathrm{MSD}^{1/2}/R^*$ as a strain. We hence remark that the threshold $\tau_c = \tau_y$ corresponds to $\mathrm{MSD}^{1/2}/R^* \simeq 10\%$, which is compatible with the macroscopic strain ($\sim$15%) needed to yield an equivalent aqueous foam at the same liquid fraction [32].

So far, we have only looked at ensemble-averaged dynamic quantities, neglecting any possible spatial fluctuation. The collapse in Fig. 3(d) might suggest that at high ϕ the dynamics is simply slowed down, so that the system does not accumulate enough stress for rearrangements to occur within the time window considered for quasi-stationarity. However, if we compare activity maps corresponding to the same MSD (but different time delays), the latter actually show a clear qualitative difference between $\phi = 65\%$ and $\phi = 80\%$, as reported in Fig. 4(a). Bubble

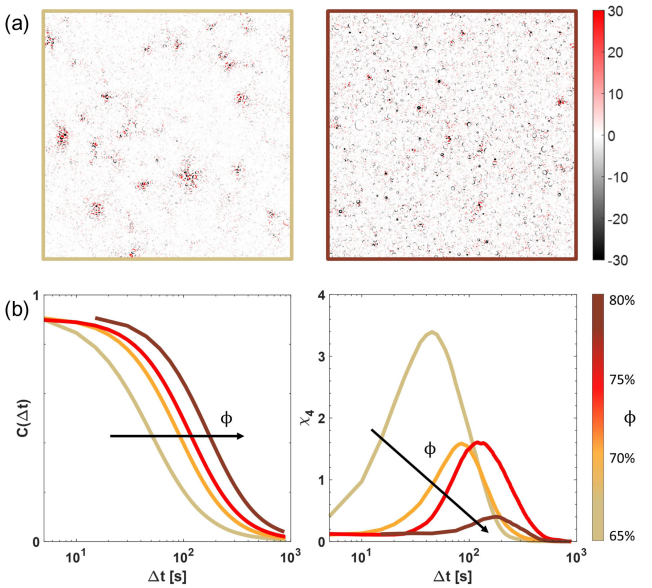

FIG. 4. Dynamic heterogeneity. (a) Examples of activity maps at time delays corresponding to the same MSD $\simeq 3 \times 10^{-4}$ mm^2 for $\phi = 65\%$ (left) and $\phi = 80\%$ (right). The edge size is 85 mm. (b) Total mobility $C(\Delta t)$ and dynamic susceptibility χ_4 for each sample.

motion is highly heterogeneous at $\phi = 65\%$, as in aqueous foams, with core regions where neighbor switching occurs surrounded by shells of bubbles that adjust at fixed topology. Such dynamic heterogeneity is lost at $\phi = 80\%$, where bubbles globally move more homogeneously.

We characterize spatial dynamic fluctuations by defining a mobility parameter that quantifies how much the bubbles move between times t and $t + \Delta t$. We define the mobility $c_i(t, \Delta t) = \exp(-|\mathbf{r}_i(t + \Delta t) - \mathbf{r}_i(t)|^2/d^2)$ for each bubble, with $d = 3\%R^*$, and compute the total mobility as the ensemble average $C(t, \Delta t) = \langle c_i(t, \Delta t)\rangle$. From the time fluctuations of the total mobility, we then evaluate the dynamic susceptibility as $\chi_4 = N(\langle C(t, \Delta t)^2\rangle - \langle C(t, \Delta t)\rangle^2)$, which efficiently measures the degree of dynamic heterogeneity [33]. Results are shown in Fig. 4(b). For each sample, χ_4 exhibits a peak at a time delay that grows with ϕ, mirroring the slowing down of the dynamics. On the other hand, the decrease of the peak height captures the loss of cooperativity and spatial correlation in bubble rearrangements at high ϕ. At high ϕ, bubbles tend to move persistently, deforming the material without relaxing the accumulated stress via neighbor-switching events. This eventually leads to the formation of unusual foam structures (SM, Fig. S6), as found with larger bubbles [13].

In conclusion, our study reveals that continuous phase rheology changes bubble dynamics in pressure-driven coarsening processes, unveiling a novel way for foams to age. The emulsion yield stress hampers bubble motion well before affecting their growth kinetics, significantly expanding our understanding of foam physics. The unexpected decoupling between bubble growth and rearrangements sheds new light on internal stress relaxation in coarsening foams, with potential implications for a broad range of aging soft glassy systems. By providing additional control on foam microstructure, our research also opens new opportunities in materials engineering and food science. As bubble organization directly impacts foam mechanical properties [34], our work can help in the design of innovative cellular materials with optimized performance [35], spanning from polymeric foams with superior impact absorption [36], to aerated dietary food products with enhanced texture and mouth feel [37,38].

Acknowledgments—The authors acknowledge Véronique Trappe for illuminating discussions. This work has been partly supported by Associazione Italiana per la Ricerca sul Cancro (AIRC) to C. G. and F. G. (MFAG#22083).

C. G., E. R., and A. S. conceptualized the experimental study. F. G. designed the methodology. C. G. conducted the experiments. C. G and F. G. analyzed the data. C. G., R. C., F. G., and A. S. interpreted the experimental results. C. G. wrote the manuscript with contributions from all authors.

[1] J. Von Neumann, *Metal Interfaces* (American Society for Metals, Cleveland, 1952).
[2] I. Cantat, S. Cohen-Addad, F. Elias, F. Graner, R. Hohler, O. Pitois, F. Rouyer, and A. Saint-Jalmes, *Foams. Structure and Dynamics* (Oxford University Press, New York, 2013).
[3] P. Sollich, F. Lequeux, P. Hébraud, and M. E. Cates, Rheology of soft glassy materials, Phys. Rev. Lett. **78**, 2020 (1997).
[4] D. J. Durian, D. A. Weitz, and D. J. Pine, Scaling behavior in shaving cream, Phys. Rev. A **44**, R7902 (1991).
[5] A. S. Gittings and D. J. Durian, Statistics of bubble rearrangement dynamics in a coarsening foam, Phys. Rev. E **78**, 066313 (2008).
[6] M. Le Merrer, S. Cohen-Addad, and R. Hohler, Bubble rearrangement duration in foams near the jamming point, Phys. Rev. Lett. **108**, 188301 (2012).
[7] D. A. Sessoms, H. Bissig, A. Duri, L. Cipelletti, and V. Trappe, Unexpected spatial distribution of bubble rearrangements in coarsening foams, Soft Matter **6**, 3030 (2010).
[8] F. Giavazzi, V. Trappe, and R. Cerbino, Multiple dynamic regimes in a coarsening foam, J. Phys. Condens. Matter **33**, 024002 (2021).
[9] M. Le Merrer, S. Cohen-Addad, and R. Hohler, Duration of bubble rearrangements in a coarsening foam probed by time-resolved diffusing-wave spectroscopy: Impact of interfacial rigidity, Phys. Rev. E **88**, 022303 (2013).
[10] H. Bey, F. Wintzenrieth, O. Ronsin, R. Hohler, and S. Cohen-Addad, Stabilization of foams by the combined effects of an insoluble gas species and gelation, Soft Matter **13**, 6816 (2017).
[11] I. Lesov, S. Tcholakova, and N. Denkov, Factors controlling the formation and stability of foams used as precursors of porous materials, J. Colloid Interface Sci. **426**, 9 (2014).
[12] B. Feneuil, P. Aimedieu, M. Scheel, J. Perrin, N. Roussel, and O. Pitois, Stability criterion for fresh cement foams, Cem. Concr. Res. **125**, 105865 (2019).
[13] C. Guidolin, J. Mac Intyre, E. Rio, A. Puisto, and A. Salonen, Viscoelastic coarsening of quasi-2d foam, Nat. Commun. **14**, 1125 (2023).
[14] T. G. Mason, J. Bibette, and D. A. Weitz, Elasticity of compressed emulsions, Phys. Rev. Lett. **75**, 2051 (1995).
[15] T. G. Mason, J. J. Bibette, and D. A. Weitz, Yielding and flow of monodisperse emulsions, J. Colloid Interface Sci. **179**, 439 (1996).
[16] J. Goyon, F. Bertrand, O. Pitois, and G. Ovarlez, Shear induced drainage in foamy yield-stress fluids, Phys. Rev. Lett. **104**, 128301 (2010).
[17] See Supplemental Material (Secs. 2 and 4) at http://link.aps.org/supplemental/10.1103/PhysRevLett.133.088202, which includes Refs. [18–23], for a short discussion on how to make drainage negligible and for quantification of directional persistency from bubble trajectories, in analogy to polymers [24].
[18] J. A. Glazier, S. P. Gross, and J. Stavans, Dynamics of two-dimensional soap froths, Phys. Rev. A **36**, 306 (1987).
[19] J. Stavans and J. A. Glazier, Soap froth revisited: Dynamic scaling in the two-dimensional froth, Phys. Rev. Lett. **62**, 1318 (1989).
[20] A. T. Chieco and D. J. Durian, Experimentally testing a generalized coarsening model for individual bubbles in

quasi-two-dimensional wet foams, Phys. Rev. E **103**, 012610 (2021).
[21] M. Pasquet, N. Galvani, O. Pitois, S. Cohen-Addad, R. Hohler, A. T Chieco, S. Dillavou, J. M. Hanlan, D. J. Durian, E. Rio, A. Salonen, and D. Langevin, Aqueous foams in microgravity, measuring bubble sizes, C. R. Méc. **351**, 139 (2023).
[22] M. Pasquet, N. Galvani, A. Requier, S. Cohen-Addad, R. Hohler, O. Pitois, E. Rio, A. Salonen, and D. Langevin, Coarsening transitions of wet liquid foams under microgravity conditions, Soft Matter **19**, 6267 (2023).
[23] N. Galvani, M. Pasquet, A. Mukherjee, A. Requier, S. Cohen-Addad, O. Pitois, R. Hohler, E. Rio, A. Salonen, D. J. Durian, and D. Langevin, Hierarchical bubble size distributions in coarsening wet liquid foams, Proc. Natl. Acad. Sci. U.S.A. **120**, e2306551120 (2023).
[24] M. Doi, S. F. Edwards, and S. F. Edwards, *The Theory of Polymer Dynamics* (Oxford University Press, New York, 1988), Vol. 73.
[25] T. Gaillard, M. Roché, C. Honorez, M. Jumeau, A. Balan, C. Jedrzejczyk, and W. Drenckhan, Controlled foam generation using cyclic diphasic flows through a constriction, Int. J. Multiphase Flow **96**, 173 (2017).
[26] C. D. Schimming and D. J. Durian, Border-crossing model for the diffusive coarsening of two-dimensional and quasi-two-dimensional wet foams, Phys. Rev. E **96**, 032805 (2017).
[27] W. W. Mullins, The statistical self-similarity hypothesis in grain-growth and particle coarsening, J. Appl. Phys. **59**, 1341 (1986).
[28] I. M. Lifshitz and V. V. Slyozov, The kinetics of precipitation from supersaturated solid solutions, J. Phys. Chem. Solids **19**, 35 (1961).
[29] J. Tinevez, N. Perry, J. Schindelin, G. M. Hoopes, G. D. Reynolds, E. Laplantine, S. Y. Bednarek, S. L. Shorte, and K. W. Eliceiri, TrackMate: An open and extensible platform for single-particle tracking, Methods **115**, 80 (2017).
[30] D. Ershov, M. Phan, J. W. Pylvanainen, S. U. Rigaud, L. Le Blanc, A. Charles-Orszag, J. R. W. Conway, R. F. Laine, N. H. Roy, D. Bonazzi, G. Duménil, G. Jacquemet, and J. Tinevez, TrackMate 7: Integrating state-of-the-art segmentation algorithms into tracking pipelines, Nat. Methods **19**, 829 (2022).
[31] J. P. Hansen and I. R. Mcdonald, *Theory of Simple Liquids* (Academic Press, London, 1986), p. 556.
[32] A. Saint-Jalmes and D. J. Durian, Vanishing elasticity for wet foams: Equivalence with emulsions and role of polydispersity, J. Rheol. **43**, 1411 (1999).
[33] L. Berthier and G. Biroli, Theoretical perspective on the glass transition and amorphous materials, Rev. Mod. Phys. **83**, 587 (2011).
[34] S. Heitkam, W. Drenckhan, T. Titscher, D. Weaire, D. C. Kreuter, D. Hajnal, F. Piechon, and J. Frohlich, Elastic properties of solid material with various arrangements of spherical voids, Eur. J. Mech. A **59**, 252 (2016).
[35] S. J. Yeo, M. J. Oh, and P. J. Yoo, Structurally controlled cellular architectures for high-performance ultra-lightweight materials, Adv. Mater. **31**, 1803670 (2019).
[36] M. Tomin and A. Kmetty, Polymer foams as advanced energy absorbing materials for sports applications—a review, J. Appl. Polym. Sci. **139**, 51714 (2022).
[37] P. R. Avallone, P. Iaccarino, N. Grizzuti, R. Pasquino, and E. Di Maio, Rheology-driven design of pizza gas foaming, Phys. Fluids **34**, 033109 (2022).
[38] S. Khemiri, N. Khelifi, M. C. Nunes, Alice Ferreira, L. Gouveia, I. Smaali, and A. Raymundo, Microalgae biomass as an additional ingredient of gluten-free bread: Dough rheology, texture quality and nutritional properties, Algal Res. **50**, 101998 (2020).